Prakash et al. 2019. *Int. J. Vehicle Structures & Systems*, 11(1), 57-63
ISSN: 0975-3060 (Print), 0975-3540 (Online)
doi: 10.4273/ijvss.11.1.11


**International Journal of Vehicle Structures & Systems**
Available online at www.maftree.org/eja

# Aerodynamics, Stability and Performance Characteristics of X-Tandem Aircrafts

**Ishaan Prakash[a] and Prithwish Mukherjee[b]**

*Dept. of Aerospace Engg., SRM University, Chennai, India*
*[a]Corresponding Author, Email: i.shaan1594@gmail.com*
*[b]Email: mukherjee.prithwish05@gmail.com*

**ABSTRACT:**

*This paper details design, analysis and validation of tandem aircraft with one wing swept forward and the other wing swept backwards. The design objective is to investigate the aerodynamic and stability characteristics of this configuration created with the motive of exploiting the manoeuvring and post stall characteristics of a forward swept wing along with the structural robustness and reliable performance of the conventional aft-swept wing. Parameters such as wing sweep, wing position, anhedral and dihedral were varied to develop a range of designs. This gave considerable information regarding the aerodynamic and stability characteristics which enabled a preliminary design of a military combat aircraft exploiting this configuration. All performance characteristics and parameters of the final design compared with current operational military aircraft give a favourable picture regarding the effectiveness of this design.*

**KEYWORDS:**

*Aircraft design; Combat aircraft; Stability; Tandem wing; Aerodynamics*

**CITATION:**

I. Prakash and P. Mukherjee. 2019. Aerodynamics, Stability and Performance Characteristics of X-Tandem Aircrafts, *Int. J. Vehicle Structures & Systems*, 11(1), 57-63. doi:10.4273/ijvss.11.1.11.

**NOMENCLATURE:**

| | |
|---|---|
| V | Velocity |
| q | Dynamic pressure |
| c | Chord length |
| b | Wing span |
| AR | Aspect Ratio |
| ρ | Density |
| $C_l$ | Coefficient of lift |
| max | Maximum |
| min | Minimum |
| η | Efficiency |
| $\frac{T}{W}$ | Thrust to weight ratio |
| TOP | Take-off parameter |
| $\frac{W}{S}$ | Wing loading |
| W | Weight in newton |
| S | Wing net platform area |
| $\sigma$ | Density ratio$\sigma = \frac{\rho_{ht}}{\rho_{MSL}}$ |
| $TO$ | Take off |
| $C_D$ | Coefficient of drag of the wing |
| $e$ | Oswal's efficiency factor |
| $C_{D0}$ | Drag at zero lift |
| $\Lambda_{LE}$ | Leading edge sweep angle |
| n | Load factor |
| M | Mach number |
| cr | Cruise |
| $\frac{L}{D}$ | Lift to drag ratio |
| a | Speed of sound |
| MSL | Mean sea level |
| ht | At cruise height |
| T | Thrust |
| req | Required |
| mp | Minimum power |
| md | Minimum drag |
| h | Vertical height above MSL |
| $\gamma$ | Glide angle |
| $\theta_c$ | Climb angle |

## 1. Introduction

The initial motivation for the proposed design rose out of sheer curiosity and efforts aimed at studying the effects on performance due to changes in configuration and placement of wings. The tandem wing configuration typically has two wings placed one behind the other. Coupling this with wing sweep, lead to the development of the proposed design. The central motive is to study the feasibility of exploiting the advantages gained due to the combined effect of both forward and reverse sweep while decreasing penalties and losses. Backward wing sweep has been traditionally used to delay onset of supersonic air flow and the accompanying wave drag so much so it has now become the norm in high speed supersonic aircraft. Forward wing speed as demonstrated by the Sukhoi-47 favours good transonic drag characteristics and low speed manoeuvrability with aero elastic tailoring being employed to compensate for wing tip deflections.

Another significant feature of the forward swept wing is that it starts to stall from the root rather than the tip providing more control at high angle of attack [1]. Hence an effort to validate the idea of exploiting the best

from both worlds has been made. The superiority of combat aircraft is measured using several parameters such as speed, weapons payload, turn rate, thrust to weight ratio, etc. Various philosophies for determining the effectiveness of such aircraft have been developed each supporting their own idea however being heavily dependent on the role of the aircraft being considered. In order to validate the effectiveness of this new configuration a design of a twin engine supersonic fighter aircraft has been done and various performance parameters and charts of present aircraft have been used as a benchmark to ensure the advantages outweigh the penalties.

## 2. Development of initial models

The very nature of the design enables several variations in wing placement. In order to fully understand the effects of such an orientation a series of different models are developed. To establish the feasibility of the design with regards to stability it is required to develop an inherently stable configuration. Longitudinal static stability requires that the slope of moment co-efficient versus angle of attack curve be negative and the centre of gravity be placed forward of the neutral point [2]. Hence a negative $C_{m\text{-}alfa\ \_}$ would be the decisive parameter for which the models would be designed. For initial studies, a homogenous mass distribution for the fuselage is assumed. The placement of the both wings is done for keeping a positive static margin and a negative slope for the $C_{m\_alfa}$ curve. Spacing between wings is kept at limits that reduce interference [3]. In order to focus on the characteristics of this wing configuration a symmetric NACA 0012 air foil, as shown in Fig. 1 is taken for the initial models for simplicity and to avoid effects due to camber.

A subsonic UAV model is developed keeping a wing aspect ratio of 5. The wing has a span of 1m and a chord of 0.2m. Due to small compressibility effects in the lower subsonic region the wing sweep angle for the forward and reverse wing are kept as (+/-) 45°. Although wing sweep is not mandatory in the subsonic regime the aim of the initial comparative study is to investigate the stability characteristics due to a forward and aft swept tandem wing. The forward swept wing is placed ahead of the fuselage C.G. and the backward swept wing is placed aft of the C.G. An initial potential flow analysis for this model is done in XFLR-5 which give a positive $C_{m\_alfa}$ curve slope. The distances of both wings are now varied by a 1mm step and analysed in each step until a negative $C_{m\_\alpha}$ slope is obtained. However with a negative$C_{m_alfa}$ slope the co-efficient of moment is required for a negative angle of attack which does not provide a positive lift. To overcome this problem an approach of introducing a tail or canard is taken.

Wing placement (High/Low/Mid), anhedral, dihedral and wing sweep are chosen as the sub-parameters which would be varied for the models. Two major families are obtained as shown in Fig. 2, one with a forward canard and the other with a rear tail. The sub-parameters are varied in each family. Taking in all possible combinations of the parameters led to a total of 40 different models each with a distinctive feature. Each model was then analysed for stability using the same procedure as applied to the initial model. Table 1 shows all the possible combinations

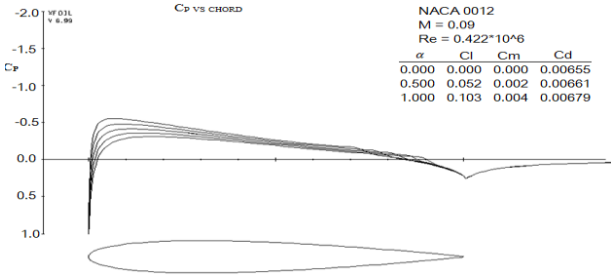


**Fig. 1: Vortex Lattice Method for NACA 0012 air foil**

**Table 1: Configurations studied**

| Main parameter (wing placement) | Sub-parameter (dihedral / anhedral (+/- 50) | Stability figure of merit | |
|---|---|---|---|
| | | Canard family | Rear tail family |
| High | None | 2 | 1 |
| | Both dihedral | 2 | 1 |
| | Both anhedral | 1 | 1 |
| | Dihedral-anhedral | 2 | 1 |
| Low | None | 2 | 1 |
| | Both dihedral | 2 | 1 |
| | Both anhedral | 1 | 1 |
| | Dihedral-anhedral | 1 | 1 |
| High-low | None | 0 | 0 |
| | Both dihedral | 0 | 0 |
| | Both anhedral | 0 | 0 |
| | Dihedral-anhedral | 0 | 0 |
| Low-high | None | 2 | 1 |
| | Both dihedral | 2 | 1 |
| | Both anhedral | 1 | 1 |
| | Dihedral-anhedral | 2 | 1 |
| Mid | None | 2 | 2 |
| | Both dihedral | 2 | 2 |
| | Both anhedral | 2 | 1 |
| | Dihedral-anhedral | 2 | 2 |

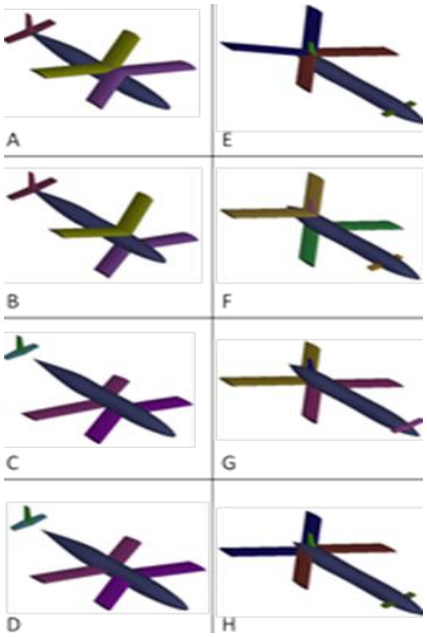


**Fig. 2: Views of developed configurations (A) High (B) Low-High (C) Low (D) Mid. (E) High (F) Low-High (G) Low (H) Mid**

## 3. Stability studies

Configurations presented in Table 1 were investigated for stability. A figure of merit rating was given based on the obtained stability results. Essentially the ease of making the configuration stable and its inherent stability characteristics were investigated. In order to achieve inherent static stability a positive static margin was kept by varying the longitudinal position of the wing in each configuration. Those configurations that were inherently stable or were easily made stable by slight re-positioning of the wings were given a rating of 2. Those which were quite challenging and required large repositioning of wings or weights to maintain a positive static margin were given a rating of 1. The high-low configuration set was rejected due to the high susceptibility of the rear wing to the downwash of the forward wing. The initial quantitative study helped in narrowing down the number of combinations needed to be investigated. The canard family showed a greater ease in achieving inherent stability. A total of 12 configurations from the canard family and 3 from the rear tail family were selected for further analysis.

### *3.1. Canard family ($C_{m\_alfa}$ curves)*

Configurations with high wings and dihedral have a higher $C_{m\_alfa}$ slope indicating high inherent stability. The HAA and HDD configurations almost coincide with each other. HDA configuration has a steeper slope compared to the HDD and H00 configurations as shown in Fig. 3. Overall the high-wing configuration seems to be less affected by changes in anhedral and dihedral angles. However when a combination of anhedral and dihedral is applied it increases the $C_{m\_alfa}$ slope. As expected the mid-wing configuration has a lower $C_{m\_alfa}$ slope. Similarly it is interesting to note that the mid-wing configuration with a dihedral and anhedral MAD has a higher $C_{m_{alfa}}$ compared to the baseline mid-wing model.

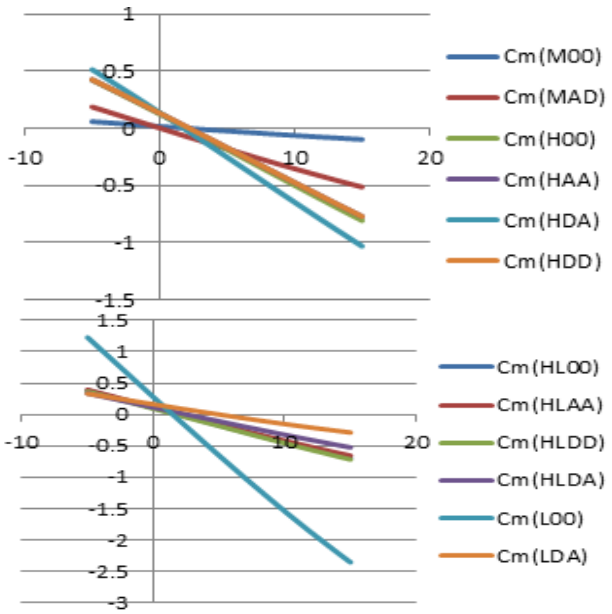


**Fig. 3: $C_{m\_alfa}$ variation for canard family (X axis: Alfa ; Y axis:Cm)**

The high-low configurations are comparatively quite flat compared to the high wing indicating reduced inherent static stability. However for the high-low configuration, application of anhedral and dihedral together decreases rather than increasing the $C_{m\_alfa}$ slope. A similar trend is observed for the low wing configuration. The highest $C_{m\_alfa}$ slope from the canard family came from the L00 configuration.

### *3.2. Tail family ($C_{m\_alfa}$ curves)*

For the tail family the mid-wing was the only configuration that gave a positive static margin while remaining under geometric constrains, Fig. 4. The MDD configuration had a quite high $C_{m\_alfa}$ slope compared to the baseline configuration. the dihedral-anhedral combination led to an increase in $C_{m\_alfa}$ slope albeit by a smaller range compared to the canard family.

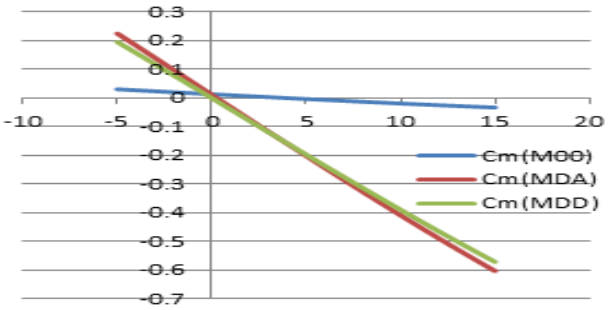


**Fig. 4:$C_{m\_alfa}$ variation for tail family (X axis: alfa; Y axis:Cm)**

### *3.3. Effect of wing sweep*

In order to study the effects of wing sweep three models were chosen from the previous study, two with almost zero $C_{m\_alfa}$ slopes and one with the highest $C_{m\_alfa}$ slope. They were the M00 cases from both families and the L00 from the canard family. For the three selected models sensitivity of co-efficient of moment to variations in wing sweep were analysed. The range of sweep angles for which the $C_{m\_alfa}$ slope remained negative is plotted in Fig. 5. The behaviour of the slope for the M00-canard configuration is quite complex with the curve achieving several peaks. However this was also the configuration which had the highest range of sweep angle within which it remained statically stable. The M00-tail configuration initially achieved a minimum peak after which it quite drastically increased becoming constant around 45 degree sweeps. The L00 configuration had a gradual decrease in the $C_{m\_alfa}$ slope reaching almost zero slope or neutral stability at around 31.2 degrees. This range in sweep angles also gives tolerance limits be required in further design.

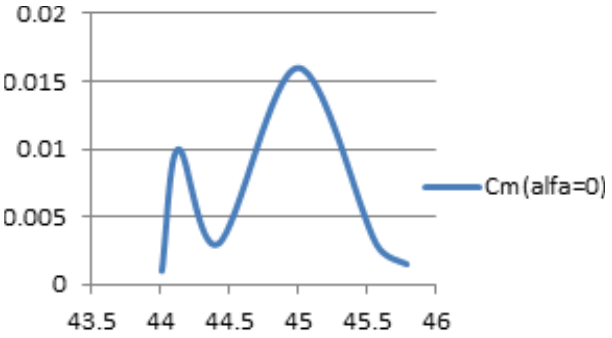


**Fig. 5(a): Effect of sweep (X-axis) variation on M00-Canard**

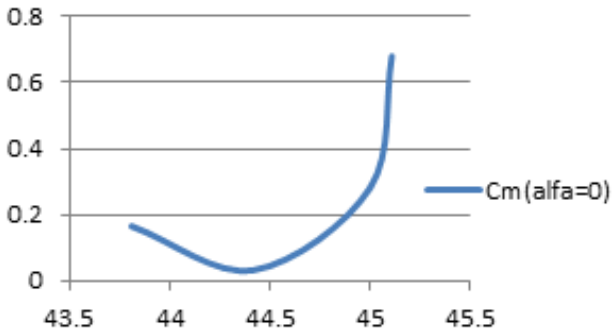


**Fig. 5(b): Effect of sweep (X-axis) variation on M00-Tail**

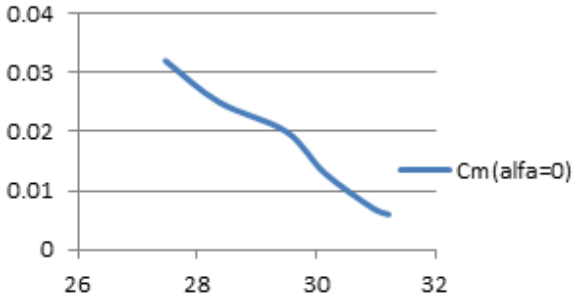


**Fig. 5(c): Effect of sweep (X-axis) variation on L00**

## 4. Fighter aircraft design formulation

In order to further validate the effectiveness of the configuration a preliminary design of a fighter aircraft with M00-canard configuration is done and expected performance parameters are to be compared with certain benchmarks. These benchmarks are obtained by a survey of current operational fighter aircraft around the world. The results of the previous comparative study are for the subsonic region and hence only used as a reference. Design of the supersonic combat aircraft is first done and a prototype is created. Later through a CFD analysis the prototype is further optimized to reflect the shockwaves during the transonic regime. A twin engine configuration is chosen to equip the aircraft with a large external carrying capacity. The design process is begun with determining a mission profile. A typical mission profile of a combat aircraft consists of take-off, cruise, dash, combat, weapons release and descent phases. Fig. 6 shows the intended mission profile for the aircraft.

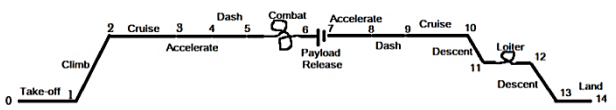


**Fig. 6: Mission profile**

Typical preliminary design techniques are utilized for the prototype. Conditions and parameters fixed from survey of current operational military aircraft are:

- Range:
  - ~ Cruise: 250 NM
  - ~ Dash: 50 NM at M=1.8
- Combat time: 3 min (M=0.8 at 20000ft)
- Loiter time: 15 min
- Maximum Mach = 2
- Acceleration: M=0.8 to M=1.4 in 30s at 35000ft
- Instantaneous turn rate >= 20 degrees/s at 350 knots at 20000ft

The design is initiated by determining wing loading and thrust to weight ratios. Wing loading for each mission segment is first calculated followed by the weight fractions for the initial sizing. Finally the total mission weight fraction is found.

### *4.1. Wing geometry*

The wing aspect ratio is given by,

$$AR = a1\ (\text{Maxi. M}^{c1}) \quad (1)$$

Where $a1 = 5.416$ ; $c1 = -0.622$ and $q = 0.5\,\rho\,V^2$ (2)

Taking $\rho$ and V at stated conditions of flight,

$$CL_{max} = CL_{cruise} + \eta\, Leadingedgeflapfactor \quad (3)$$

All formulation and required empirical results used for initial preliminary design is taken from [4-5]. Vortex Lattice method analysis of the NACA 63206 airfoil is shown in Fig. 7.

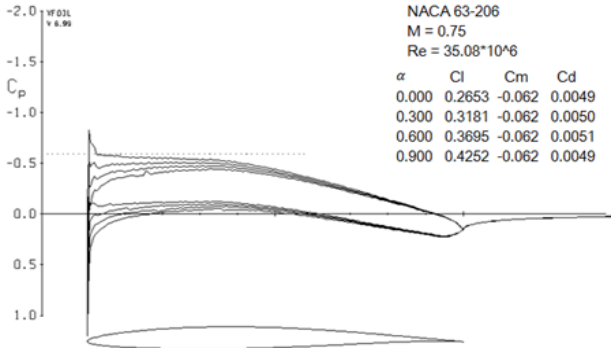


**Fig. 7: Vortex Lattice method analysis of the NACA 63206 airfoil**

### *4.2. Wing loading and thrust to weight ratios*

The wing loading (WL) parameter is found for all mission segments using following equations.

$$WL_{\text{take\_off}} = \frac{CL_{max}\,\frac{T}{W}\,TOP}{1.21} \quad (4)$$

$$TOP = \frac{\frac{W}{S}}{\sigma\, CL_{TO}\,\frac{T}{W}} \quad (5)$$

$$WL_{Landing} = \frac{CL_{max}\,S_g}{80} \quad (6)$$

$$\sigma = \frac{\rho_x}{\rho_0} \quad (7)$$

$S_g$ = 300 m (landing ground roll) (8)

$$\text{WL}_{cruise} = q_{cruise}\sqrt{\frac{\pi\, AR\, e\, C_D}{3}} \quad (9)$$

$$C_D = C_{D0} + K\, CL^2 \quad (10)$$

$$K = \frac{1}{\pi e\, AR} \quad (11)$$

Oswal's efficiency factor [6] is given by,

$$e = 4.61\left(1 - (0.045\, AR^{0.68})\right)\cos(\Lambda_{LE})^{0.15} - 3.1 \quad (12)$$

$$WL_{maneuver} = \frac{q_i\, CL_{manuever}}{n_{limit}} \quad (13)$$

$$n_{limit} = \sqrt{\left(\frac{Vi\ turnrate}{g}\right)^2 + 1} \quad (14)$$

$$\text{WL}_{maneuver_{eff}} = \frac{WL_{maneuver}}{0.85} \quad (15)$$

$$WL_{turn} = \frac{\frac{T}{W_{turn}} + \sqrt{\frac{T}{W_{turn}}^2 - \frac{4\times 5^2 C_D}{\pi\, AR\, e(turn)}}}{\frac{2\times 5^2}{q_{st}\,\pi\, AR\, e_{turn}}} \quad (16)$$

$$e_{turn} = e - 0.3e \quad (17)$$

$$WL_{combat} = WL_{stall} \times 0.85 \quad (18)$$

$$\frac{T}{W_{combat}} = \frac{q_{st}\, C_d}{WL_{combat}} + WL_{combat}\, \frac{5^2}{q_{st}\, \pi\, AR\, e_{turn}} \quad (19)$$

$$\frac{T}{W_{take\_off}} = \frac{T}{W_{combat}}\, 0.85\, \frac{30000}{16000} \quad (20)$$

### *4.3. Initial sizing; mission weight fractions*

$$We_0 = a3 + b\, W_0^{c3}\, AR^{c4}\, \left(\frac{T}{W}^{c5}\right)_{takeo\_ff} \quad (21)$$

$$WL_{cr2} = WL_{stall}\, W_{01}\, W_{12} \quad (22)$$

$$W_{01} = 0.98$$

$$W_{12} = 1.0065 - 0.0325\ M_{cr} \quad (23)$$

$$\frac{L}{D_{cr}} = \frac{1}{\frac{q_{cr}\, C_D}{WL_{cr2}} + \frac{WL_{cr2}}{q_{cr}\, \pi\, AR\, e}} \quad (24)$$

$$W_{23} = \exp - \frac{0.94 \times 1.519 \times 10^6}{876\, \frac{L}{D_{cr}}\, 3600} \quad (25)$$

$$W_{34} = 0.9764\ ;\ M_{dash} = 1.8$$

$$V_{dash} = M_{dash}\, a \quad (26)$$

$$q_{dash} = \frac{1}{2}\, \rho_{35}\, V_d^2 \quad (27)$$

$$WL_{dash} = WL_{stall}\, W_{01}\, W_{12}\, W_{23}\, W_{34} \quad (28)$$

$$\frac{L}{D_{dash}} = \frac{1}{\frac{q_{dash}\, CD_{0_{dash}}}{WL_{dash}} + \frac{WL_{dash}\, k}{q_{dash}}} \quad (29)$$

$$W_{45} = \exp \frac{-50 \times 6076 \times 1.06}{V_{dash}\, \frac{L}{D_{dash}}\, 3600} \quad (30)$$

$$\frac{T}{W_{combat_2}} = \frac{\frac{T}{W_{take_{off}}}^{\frac{16}{30}}}{W_{01}\, W_{12}\, W_{23}\, W_{34}\, W_{45}} \quad (31)$$

$$W_{56} = 1 - \frac{1.57\, \frac{T}{W_{combat_2}}\, \text{x}3 \times 60}{3600} \quad (32)$$

$$W_{11\_12} = 0.993; W_{13\_14} = 0.995$$

$$WL_{loiter} = WL_{stall}\, W_{01}\, W_{12}\, W_{23}\, W_{34}\, W_{45}\, W_{56}\, W_{34}$$

$$W_{45}\ W_{23}\, W_{11\_12} \quad (33)$$

$$V_{loiter} = \sqrt{\frac{2\, WL_{loiter}}{\rho}\, \sqrt{\frac{1}{C_D\, \pi\, AR\, e}}} \quad (34)$$

$$\frac{L}{D_{loiter}} = \frac{1}{\frac{q_{loiter}\, C_D}{WL_{loiter}} + \frac{WL_{loiter}}{q_{loiter}\, \pi\, AR\, e}} \quad (35)$$

$$W_{12\_13} = \exp \frac{-15 \times 60 \times 0.906}{\frac{L}{D_{loiter}} \times 3600} \quad (36)$$

### *4.4. Final weight fractions*

$$W_{0_{14}} = W_{0_1}\, W_{1_2}\, W_{2_3}\, W_{3_4}\, W_{4_5}\, W_{5_6}\, W_{3_4}\, W_{4_5}\ W_{2_3}\, W_{11_{12}}\ W_{12\_13}\, W_{13\_14} \quad (37)$$

$$W_{f0} = 1.04\, (1 - W_{0\_14}) \quad (38)$$

Taking the obtained values the final sizing iterations gave the results as shown in Table 2.External Fuel tanks and possible weapons payload are carried by 17 hard-points as follows:

- 2 External fuel tanks (2760 kg each of fuel)
- 10 air to air (light) ~ 200 kg each
- 4 air to surface (heavy & medium) ~ 100 kg each
- 1 Heavy weight Long range missile (Eg.: Brahmos) = 2500 kg
  - ~ without heavy weight missile : 8*(air to air) and 4*(air to surface)
  - ~ With heavy weight missile : 8*(air to air) and 3*(air to surface)

**Table 2: Preliminary design results**

| Parameter | Value |
|---|---|
| Aspect ratio | 3.52 |
| Span | 9.25 m |
| Mean chord | 6.04 m |
| Wing area | 97.4 $m^2$ |
| Fuselage length | 21.68 m |
| Coefficient of lift (max) | 1.41 |
| Coefficient of drag of the wing | 0.015 |
| Lift to drag ratio (cruise) | 10.29 |
| Lift to drag ratio (dash) | 0.595 |
| Lift to drag ratio (loiter) | 11.35 |
| Mach number (cruise) | 0.75 |
| Mach number (dash) | 1.8 |
| Thrust to weight ratio (take-off) | 1.25 |
| Thrust to weight ratio (combat) | 0.83 |
| Wing loading (max) | 64.43 |
| Wing loading (cruise) | 61.7 |
| Wing loading (dash) | 57.65 |
| Wing loading (loiter) | 42.09 |
| Total weight | 30642 kg |
| Empty weight | 12770 kg |
| Payload weight (external fuel tank + ordnance) | 7574 kg |

### *4.5. Performance parameters*

From the designed aircraft several important performance parameters are now estimated.

#### 4.5.1. Straight and level flight

$$a = \sqrt{\gamma\, R\, T_{ht}} \quad (39)$$

$$\sigma = \frac{\rho_{ht}}{\rho_{MSL}} \quad (40)$$

$$V_{MSL} = \frac{V_{ht}}{\sqrt{\sigma}} \quad (41)$$

Parameters at altitude:

$$Cl_{ht} = \sqrt{\frac{2\, W_{23}}{\rho_{ht}\, S\, V_{ht}^2}} \quad (42)$$

$$Cd_{ht} = Cd_0 + K\, CL_{ht}^2 \quad (43)$$

$$V_{ht} = \sqrt{\frac{2\, W_{23}}{\rho_{ht}\, S\, Cl_{ht}}} \quad (44)$$

$$\frac{L}{D_{ht}} = \frac{CL_{ht}}{CD_{ht}} \quad (45)$$

$$D_{ht} = W_{23}\, \frac{1}{\frac{L}{D_{ht}}} \quad (46)$$

$$T_{req} = D_{ht} \quad (47)$$

$$L_{ht} = \frac{1}{2}\, \rho_{ht}\, {V_{ht}}^2\, S\, Cl_{ht} \quad (48)$$

$$\frac{L}{D_{max}} = \frac{1}{2\sqrt{K\, Cd_0}} \quad (49)$$

$$V_{md} = \sqrt{\frac{2\, W_{23}}{\rho_{ht}\, S}}\, \sqrt[4]{\frac{K}{Cd_0}} \quad (50)$$

$$V_{mp} = \sqrt{\frac{2\, W_{23}}{\rho_{ht}\, S}}\, \sqrt[4]{\frac{K}{3\, Cd_0}} \quad (51)$$

$$\frac{L}{D_{mp}} = 0.866 \frac{L}{D_{max}} \quad (52)$$

#### 4.5.2. Gliding

$$\gamma = \tan^{-1} \frac{1}{\frac{L}{D_{ht}}} \quad (53)$$

$$Range = h \frac{L}{D_{ht}} \quad (54)$$

$$V_{sinking} = V_{ht} \sin(\gamma) \quad (55)$$

$$Time_{sinking} = \frac{h}{V_{sinking}} \quad (56)$$

#### 4.5.3. Climbing

$$\theta_c = \sin^{-1}\left(\frac{T_{av}-T_{req}}{W}\right) \quad (57)$$

$$Rate of Climb = V_{MSL} \sin(\theta_c) \quad (58)$$

$$n = \frac{Lift_{ht}}{W} \quad (59)$$

The important results obtained for the performance parameters are given in Table 3.

**Table 3: Performance parameters**

| Parameter | Value | Parameter | Value |
|---|---|---|---|
| $V_{MSL}$ | 399.5865 m/s | $(L/D)_{mp}$ | 9.8384 |
| $Cl_{ht}$ | 0.3 | $\gamma$ | 5.0866° |
| $Cd_{ht}$ | 0.026 | $V_{sinking}$ | 19.725 m/s |
| $V_{ht}$ | 222.38 m/s | $Time_{sinking}$ | 542.85 s |
| $T_{req}$ | 23823 N | $\theta_c$ | 48.2058° |
| $V_{md}$ | 218.414 m/s | $Rate\ of\ Climb$ | 297.999 m/s |
| $V_{mp}$ | 165.96 m/s | $n$ | 0.89 |
| $(L/D)_{ht}$ | 11.538 | | |

Once the preliminary design is complete a potential flow model is developed as shown in Fig. 8. Using the dimensions obtained from the wing design a full scale wing is modelled. The fuselage is not included in the potential flow analysis to cancel out interference which may not be properly calculated. The weight of the fuselage is equally distributed in the forward and backward wings. In order to simulate the weight of the engines the vertical stabilizers are given the equivalent engine weight for simplicity it is assumed that the centre of gravity for the vertical tail and engines coincide. Fuel weight is also distributed in the wings. Crew weight is given at the canards due to their proximity to the cockpit. This model is analysed for determining the aerodynamic and stability characteristics of the designed aircraft. The same iterative process developed during the comparative study the wing placement is chosen so as to provide a longitudinal stability to enable good manoeuvrability. The iterations are performed to get a near neutral static stability condition i.e. the condition when centre of gravity and neutral point coincide as depicted in Fig. 9.

The $C_{m\_alfa}$ curve shows almost zero slope value. There is a slightly negative slope from 0 to 5° angle of attack and a slightly positive slope from 0 to 10°. There is however a nose down pitching moment being almost independent of angle of attack. This relaxed stability condition is taken to provide improved manoeuvrability. A robust fly by wire control would be required for optimum performance owing to the nose down pitching moment. Using the geometrical co-ordinates obtained from the final potential flow model a CAD prototype, as shown in Fig. 10, is developed exactly to scale in order to enable an accurate CFD analysis for the final design. This is needed to validate the surface pressure distribution, Mach number, lift and drag co-efficient. CFD analysis is not limited by geometric or flow properties [7]. Using CFD, an analysis is performed to determine and ensure a favourable Mach number and pressure distribution on the surface. The finalized potential flow model co-ordinates are exported to develop a prototype for the CFD analysis. A refined mesh is used to capture the intended surface parameters.

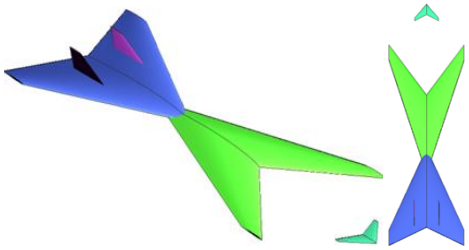

**Fig. 8: Potential flow prototype**

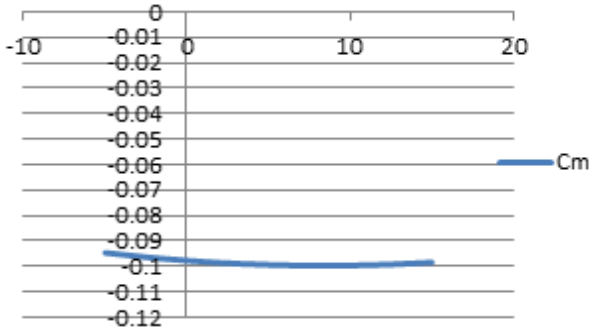


**Fig. 9(a):$C_{m\_alfa}$ vs. Angle of attack**

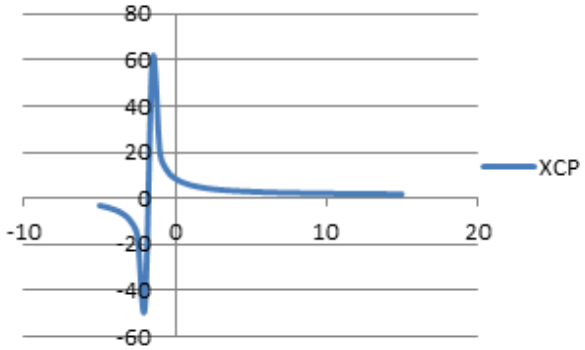


**Fig. 9(b):Xcp (Centre of pressure) Position vs. Angle of attack**

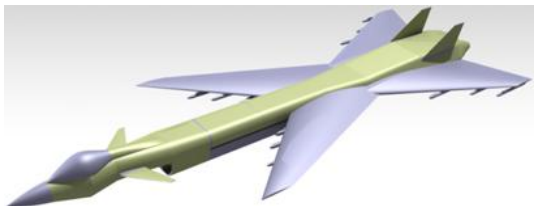

**Fig. 10: CAD prototype**

## 5. Results and discussions

After an extensive study two families of favourable configurations were developed utilizing a canard and rear tail respectively. It is established that the canard family is much easier to stabilize and the low wing configuration gives the steepest $C_{m\_alfa}$ slope. With regards to high and neutral static longitudinal stability

three models were identified as shown in Fig. 11. A twin engine supersonic fighter exploiting the proposed configuration was developed and performance parameters were calculated. A comparison of the obtained parameters and current operational fighter aircraft has been made in Table 4. The surface pressure and Mach number distribution on the wings and canards were analysed using CFD. The resulting contours are shown in Fig. 12. The area where the two wings merged was the point of interest. At dash velocity the local Mach in this region does not increase drastically. This can also be inferred from the smooth transition of pressure contours in this region. More importantly the presence of the fuselage will ensure that the inward span-wise flow of the forward wings never meets.

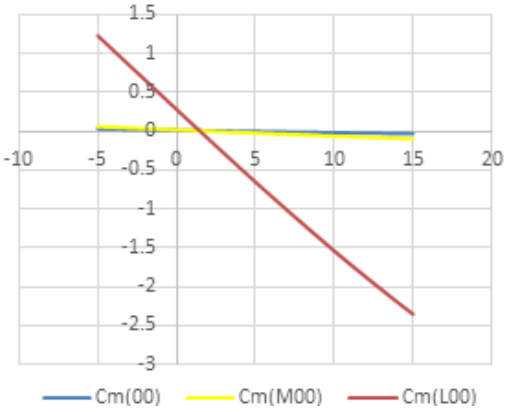


**Fig. 11: Moment co-efficient variation of selected configurations**

**Table 4: Comparisons with some operational aircrafts**

| Parameter | F-15 | F-16 | F/A-18 | X-29A | Rafale | Su-30 | X-Wing |
|---|---|---|---|---|---|---|---|
| Aspect ratio | 3.01 | 3.09 | 4 | 4 | 2.6 | 3.5 | 3.52 |
| Wing area($m^2$) | 56.48 | 27.88 | 46.3 | 17.46 | 46 | 62 | 97.4 |
| MTOW (kg) | 36700 | 19187 | 29937 | 8074 | 24500 | 38800 | 30642 |
| Lift induced drag | 0.0218 | 0.0199 | 0.0239 | 0.0276 | NA | NA | 0.0298 |
| L/D (subsonic) | 8.6 | 10.1 | 9.8 | 9 | NA | NA | 11.35 |
| Range (km) | 1853 | 860 | 740 | 560 | NA | 1500 | 1480 |
| Rate of climb(m/s) | >254 | ~254 | >228.6 | NA | 304.8 | 280 | 298 |
| T/W | 1.19 | 1.06 | 1.09 | NA | 1.16 | 1.14 | 1.46 |

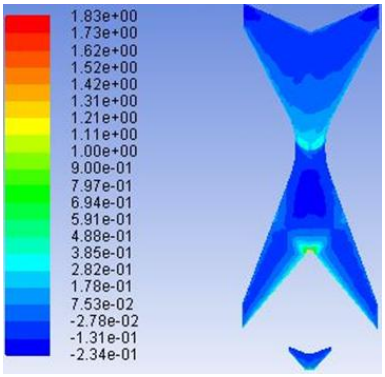


**Fig. 12(a): Pressure co-efficient contour**

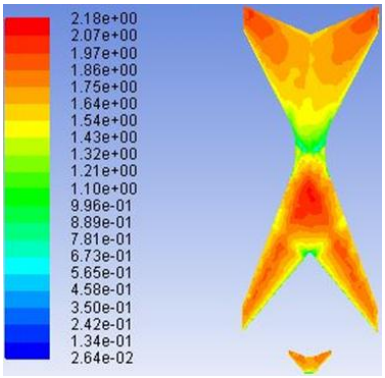


**Fig. 12(b): Skin friction co-efficient contour**

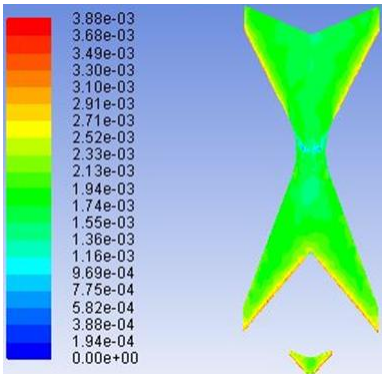


**Fig. 12(c): Mach number contour**

## 6. Conclusion

This study demonstrated that the proposed x-tandem configuration has potential to be adopted in aircraft design. The aerodynamic and stability characteristics of the configuration were extensively studied for small scale and large scale applications in both subsonic and supersonic regimes. We can conclude that the proposed configuration can be used in military fighter aircrafts or unmanned aerial vehicles where there is a need for manoeuvrability and an increased payload capacity.

### REFERENCES:

[1] W.P. Honderson and J.K. Huffman. 1975. Aero-dynamic characteristics of a tandem wing configuration at a mach number of 0.30, *NASA Tech. Memorandum X-72779*.

[2] L.T. Nguyen, M.E. Ogburn, W.P. Gilbert, K.S. Kibler, P.W. Brown and P.L. Deal. 1979. Simulator study of stall/post-stall characteristics of a fighter airplane with relaxed longitudinal static stability, *NASA Tech. Paper* 1538.

[3] T.M. Broering and Y. Lian. 2010. The effect of wing spacing on tandem wing aerodynamics, *Proc. 28th AIAA Applied Aerodynamics Conf.*, Chicago, Illinois. https://doi.org/10.2514/6.2010-4385.

[4] D.P. Raymer. 1992. *Aircraft Design: A Conceptual Approach*, 2nd Ed., AIAA Educational Series.

[5] O. Gur, W.H. Mason and J.A. Schetz. 2010. Full configuration drag estimation, *J. Aircraft*, 47(4), 1356-1367. https://doi.org/10.2514/1.47557.

[6] Kroo. 2005. Non-planar wing concepts for increased aircraft efficiency, *VKI Lecture Series on Innovative Configurations and Advanced Concepts for Future Civil Aircraft*, 1-29.

[7] W.C. Moonan. 2010. *Evaluation of the Aerodynamics of an Aircraft Fuselage Pod Using Analytical, CFD, and Flight Testing Techniques*, Master Thesis, University of Tennesse, Knoxville.

[8] E.J. Saltzman and J.W. Hicks. 1994. In-flight lift-drag characteristics for a forward-swept wing aircraft (and comparisons with contemporary aircraft), *NASA Technical Paper 3414*.